






RESEARCH ARTICLE | FEBRUARY 05 2024

# Designable and unidirectional motion of Leidenfrost droplets on heated asymmetric microgrooves written by femtosecond laser **EP FREE**

Zilong Cheng; Chaowei Wang ; Xinlei Li ; Tianyu Xu; Zhenrui Chen; Zehang Cui; Kangru Cheng; Suwan Zhu ; Dong Wu ; Jiale Yong 

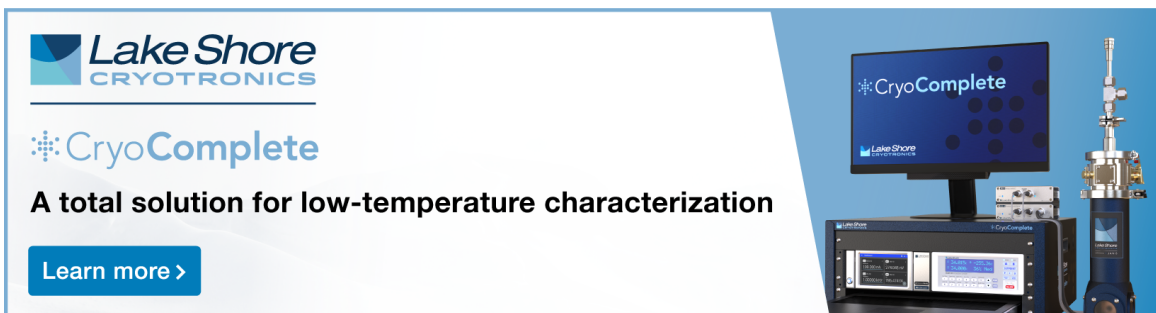
 Check for updates

*Appl. Phys. Lett.* 124, 061601 (2024)

<https://doi.org/10.1063/5.0187674>



CrossMark



**Lake Shore**  
CRYOTRONICS

**CryoComplete**

**A total solution for low-temperature characterization**

[Learn more >](#)

The advertisement features a photograph of the CryoComplete system, which includes a computer monitor displaying the software interface, a control unit, and a cryogenic probe assembly.

# Designable and unidirectional motion of Leidenfrost droplets on heated asymmetric microgrooves written by femtosecond laser

Cite as: Appl. Phys. Lett. **124**, 061601 (2024); doi: [10.1063/5.0187674](https://doi.org/10.1063/5.0187674)

Submitted: 15 November 2023 · Accepted: 12 January 2024 ·

Published Online: 5 February 2024



View Online



Export Citation



CrossMark

Zilong Cheng, Chaowei Wang,<sup>a)</sup>  Xinlei Li,  Tianyu Xu, Zhenrui Chen, Zehang Cui, Kangru Cheng, Suwan Zhu,  Dong Wu,  and Jiale Yong<sup>a)</sup> 

## AFFILIATIONS

CAS Key Laboratory of Mechanical Behavior and Design of Materials, Department of Precision Machinery and Precision Instrumentation, University of Science and Technology of China, Hefei 230027, People's Republic of China

<sup>a)</sup> Authors to whom correspondence should be addressed: [chaoweiw@ustc.edu.cn](mailto:chaoweiw@ustc.edu.cn) and [jlyong@ustc.edu.cn](mailto:jlyong@ustc.edu.cn)

## ABSTRACT

Unidirectional droplet motion is realized on heated asymmetric microgroove arrays prepared by femtosecond laser direct writing. The plasma expansion under laser ablation compresses the two sides of the induced microgroove differently, resulting in the formation of asymmetrical microgrooves. The asymmetry of the microgrooves can rectify the water vapor that ejects from the Leidenfrost droplet and generate a viscous shear force at the bottom of the droplet, causing the droplet to move in a certain direction (where the laser scanning line is added) when the substrate temperature is higher than a certain critical value (the transition temperature of disordered motion and unidirectional motion). The velocity of droplets can exceed 318 mm/s, and the droplets can even climb surfaces that are tilted 14°. With the advantages of femtosecond lasers in the flexible design of surface microstructures and patterns, this unidirectional droplet motion can support a variety of complex droplet-manipulation applications, such as droplet movement along designed trajectories, droplet accelerator devices, fixed-point capture of droplets, and fixed-point cooling of hot solid surfaces. Compared with traditional macroscopic ratchets, laser-written asymmetrical microgrooves make the Leidenfrost droplet motion more designable and controllable.

Published under an exclusive license by AIP Publishing. <https://doi.org/10.1063/5.0187674>

Controlled propulsion of liquid droplets on a solid surface not only generates fascinating science but also plays a critical role in various applications ranging from fluidic processing to thermal management.<sup>1–3</sup> To achieve directional and fast droplet motion, it is necessary to break the wetting symmetry of the droplet on a surface, which is usually achieved with the help of external driving forces (e.g., light,<sup>4,5</sup> temperature,<sup>6,7</sup> electricity,<sup>8</sup> and mechanical vibration<sup>9,10</sup>) or by designing topological/chemical gradients on the substrate surface.<sup>11,12</sup> Although the gradient structure can realize spontaneous directional movement of droplets, the transport distance is usually very short (usually a few centimeters) because of the tradeoff of hydrodynamics (as the gradient generally weakens).<sup>13,14</sup> A fascinating phenomenon called the Leidenfrost effect occurs when the solid substrate supporting the droplet is above a critical temperature. A continuous vapor layer forms between the droplet and substrate because of heat-induced evaporation, which separates the droplet from the hot solid surface and eliminates the pinning of the contact line.<sup>15,16</sup> The Leidenfrost droplets on the heated surface will spontaneously push forward, but in an

arbitrary random direction (i.e., an isotropic self-propelled process). Generally, the motion direction of the Leidenfrost droplet can be controlled by the macroscopic three-dimensional (3D) ratchet structures obtained by mechanical processing [Fig. 1(a)]. The asymmetry of the ratchet structure can rectify the water vapor at the bottom of the droplet and make the Leidenfrost droplets move spontaneously and in a unidirectional manner.<sup>17–21</sup> However, the preparation of macroscopic ratchet structures not only removes a large amount of material on the substrate surface but also makes the surface visible to the naked eye uneven. This is not allowed in many applications. Moreover, the macroscopic ratchet is difficult to form complex shapes by machining methods, so the movement direction of the Leidenfrost droplets is not easy to design and control. Therefore, a simpler and more effective method to achieve designable and unidirectional Leidenfrost droplet motion than the traditional macroscopic ratchet structure is still worth looking forward to.

In this Letter, we find that droplets are capable of unidirectional motion on heated asymmetric microgroove arrays that are directly

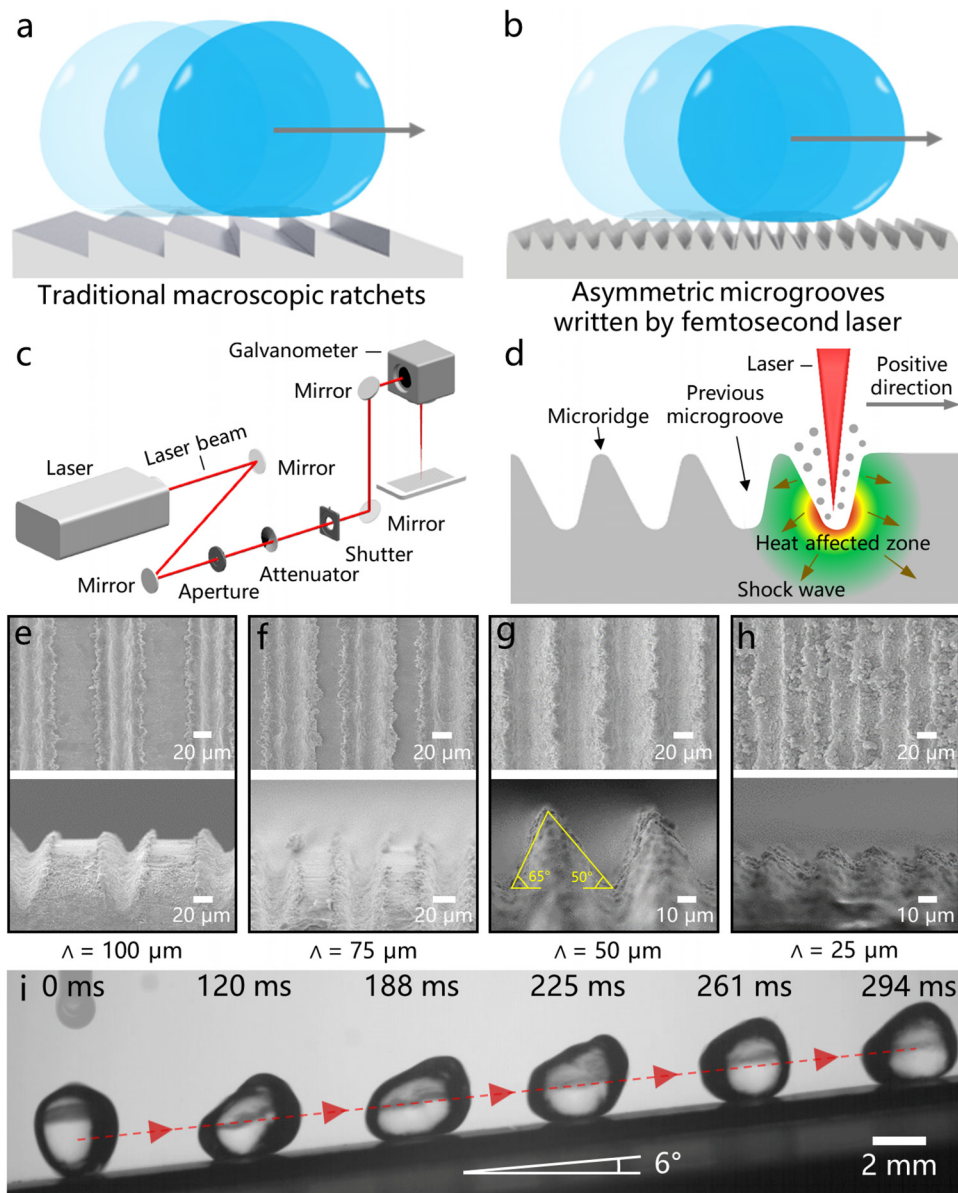


**FIG. 1.** Unidirectional droplet motion and the preparation of asymmetric microgrooves by a femtosecond laser. (a) Unidirectional transport of droplets on the traditional macroscopic ratchets in a thermal environment. (b) Unidirectional transport of droplets on the heated asymmetric microgrooves. (c) Femtosecond laser processing system. (d) Formation mechanism of the asymmetric microgrooves by femtosecond laser processing. (e)–(h) Top- and side-view SEM images of the laser-induced microgrooves with different intervals ( $\Lambda$ ). (i) Time-lapse trajectory of the Leidenfrost droplet climbing up the inclined surface. Multimedia available online.

written by a femtosecond laser [Fig. 1(b)]. The influences of substrate temperature, period of the microgroove array, droplet volume, tilt angle, and Weber number on the droplet's kinetic behavior on the asymmetric microgrooves were carefully investigated. Combined with the flexibility of the femtosecond laser in the design of surface microstructures and patterns, this spontaneous and unidirectional droplet motion can support various complex droplet manipulation applications.

The asymmetric microgroove array was simply prepared by femtosecond laser direct writing. As shown in Fig. 1(c), the femtosecond laser beam (wavelength = 800 nm, pulse duration = 104 fs, and repetition rate = 1 kHz) was guided into a galvanometer scanner and focused onto the surface of Al sheets (thickness = 1 mm) by an  $f$ - $\theta$  lens (focal length = 63 mm). A typical line-by-line scanning method

was adopted to produce a microgroove array [Fig. 1(d)].<sup>22–25</sup> The direction in which the laser scanning lines are added is defined as the positive direction. Figures 1(e)–1(h) show the scanning electron microscopy (SEM) images of the laser-induced microstructures. An individual scanning line can generate a microgroove with a width of  $\sim 53$  and a depth of  $\sim 38$   $\mu\text{m}$  at a laser power of 250 mW and a scanning speed of 2 mm/s. As the scanning interval ( $\Lambda$ ) decreases, the laser-induced microgrooves get closer, and the smooth area between adjacent grooves also decreases. When  $\Lambda$  is reduced to 50  $\mu\text{m}$ , the microgrooves slightly overlap, and microridges form between the microgrooves [Fig. 1(g)]. Interestingly, the microridges tilt slightly in the opposite direction where the laser scanning lines are added, presenting a certain degree of asymmetry. It is found that the asymmetric

microgrooves can be obtained only when the scanning interval is slightly smaller than the width of a single microgroove. When droplets are dropped on the heated surface with asymmetric microgrooves at 300 °C, all droplets will move at high speed along the positive direction, showing a unidirectional movement characteristic [Fig. 1(i), Movie S1 in Multimedia available online].

The formation mechanism of asymmetric microgrooves is shown in Fig. 1(d). Under femtosecond laser ablation, the generated ultrahigh temperature of the plasma causes the laser-processed region to be in a transient melting state. Meanwhile, the plasma with ultrahigh pressure exerts an extremely strong pressure force on both sides of the laser-induced grooves.<sup>26–32</sup> When  $\Lambda$  is close to the width of the laser-induced microgroove, the previous side of the laser-written line is a laser-induced microgroove, while the other side is the unablated smooth substrate. The micridge between the currently formed microgroove and the previous microgroove is more likely to be squeezed by the plasma and, thus, tilt toward the previous microgroove. Therefore, asymmetric microgrooves are finally obtained through line-by-line laser writing (see the supplementary material for more details).

Figure 2 and Movie S2 (Multimedia available online) show the dynamic behavior of water droplets on the heated smooth Al surface (without laser treatment) at different temperatures. As the temperature increases, the droplets exhibit four different states: droplet firmly

adhering to the smooth surface (the single-phase state) [Fig. 2(a)], nucleate boiling state [Fig. 2(b)], transition boiling state [Fig. 2(c)], and film boiling state (the Leidenfrost state) [Fig. 2(d)].<sup>33–38</sup> In the single-phase state, the droplets firmly adhere to the smooth surface. Since the evaporation process only occurs at the liquid–gas interface, the whole evaporation process is relatively slow. The droplets will slowly evaporate *in situ* within 290 s ( $T = 120$  °C). When  $T$  rises to 160 °C, exceeding the trigger temperature of nuclear boiling, the droplet explodes immediately and produces a large number of tiny splashed droplets upon contact with the Al surface. At this temperature, the droplet is in a nucleated boiling state, and the evaporation process is extremely rapid. The droplet can evaporate completely in 840 ms. As  $T$  further increases from 160 to 200 °C, the droplet gradually changes from the nucleate boiling state to the transition boiling state. In the transition boiling state, the vapor generated underneath the droplet can lift the droplet partially away from the surface, and tiny droplets are still produced and sputtered. Different from the rapid evaporation of droplets in the nucleate boiling state, the droplet in the transition boiling state can move freely and randomly on the surface. When  $T$  rises beyond the critical film boiling temperature, the droplets enter the film boiling state, that is, the Leidenfrost effect. The water vapor layer completely separates the droplets from the aluminum surface. The droplet can be stably suspended on the smooth aluminum plate for a long time, maintaining a complete spherical shape. Since the droplet is not subject to

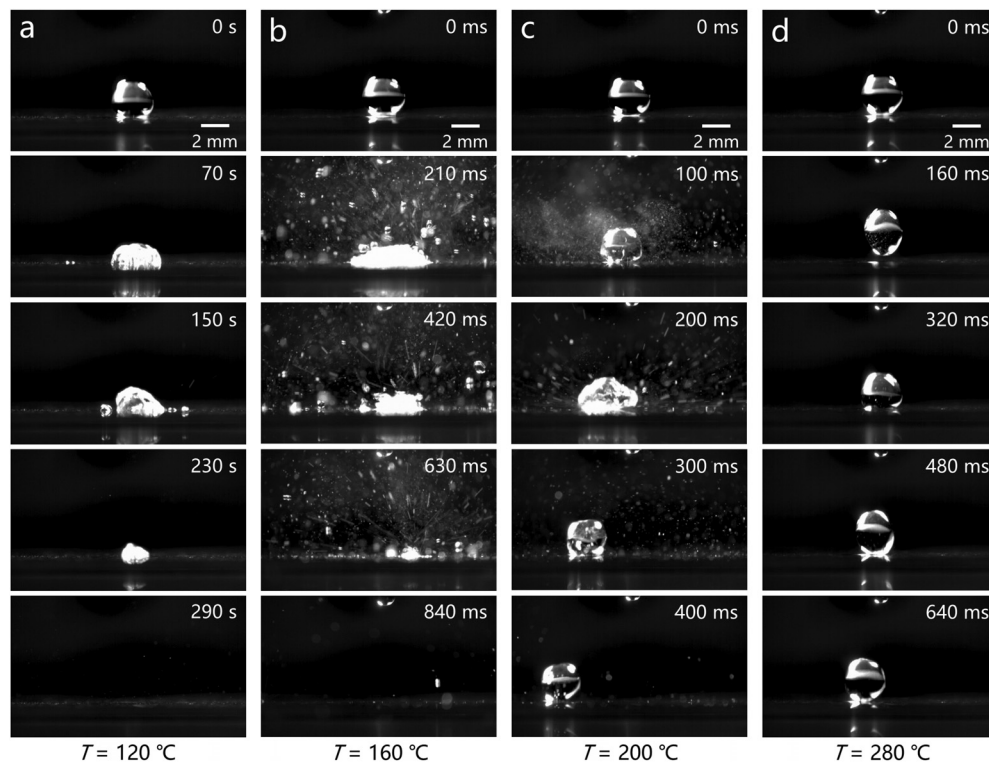


**FIG. 2.** Dynamic behavior of a droplet on a heated smooth Al surface at different temperatures. (a) Water droplet in the single phase state evaporating slowly at 120 °C. The droplet evaporated completely within 290 s *in situ*. (b) Water droplet in the nucleate boiling state and spraying rapidly at 160 °C. The droplet evaporated completely within 840 ms *in situ*. (c) Water droplet in the transition boiling state and rolling randomly at 200 °C. (d) Water droplet entering the film boiling state and being suspended on the substrate at 280 °C. Multimedia available online.



adhesion, it will move freely on the heated surface. Although the temperature variation alters the boiling state of droplets, the direction of droplet motion is random in the transition boiling and film boiling states (Movie S3 in the supplementary material). Thus, on a heated nontextured surface, the movement of droplets is nondirectional. The effect of homogeneous surface micro/nanostructures on the dynamic behavior of liquid droplet on the heated Al surface was also investigated, as shown in Fig. S1 and Movie S4 (supplementary material). The droplet's behavior on the nanostructured surface is similar to that on the nonablated smooth aluminum surface. Droplets also cannot move unidirectionally on such a surface, which is mainly due to the

homogeneity and isotropy of the laser-induced nanostructures (see the supplementary material for more details).

Figures 3(a)–3(d) and Movie S5 (Multimedia available online) show the droplet behavior on the laser-induced periodic asymmetric microgrooves at different temperatures. At low temperatures, droplets adhere to the surface and slowly evaporate. When the temperature rises to 170 °C [Fig. 3(a)], the droplet is in a nucleate boiling state and evaporates rapidly within a few hundred milliseconds. In this state, the droplet still cannot move on the surface. When the temperature increases to 230 °C, the droplet reaches a transition boiling state, and its bottom partially touches the microgroove [Fig. 3(b)]. The tiny

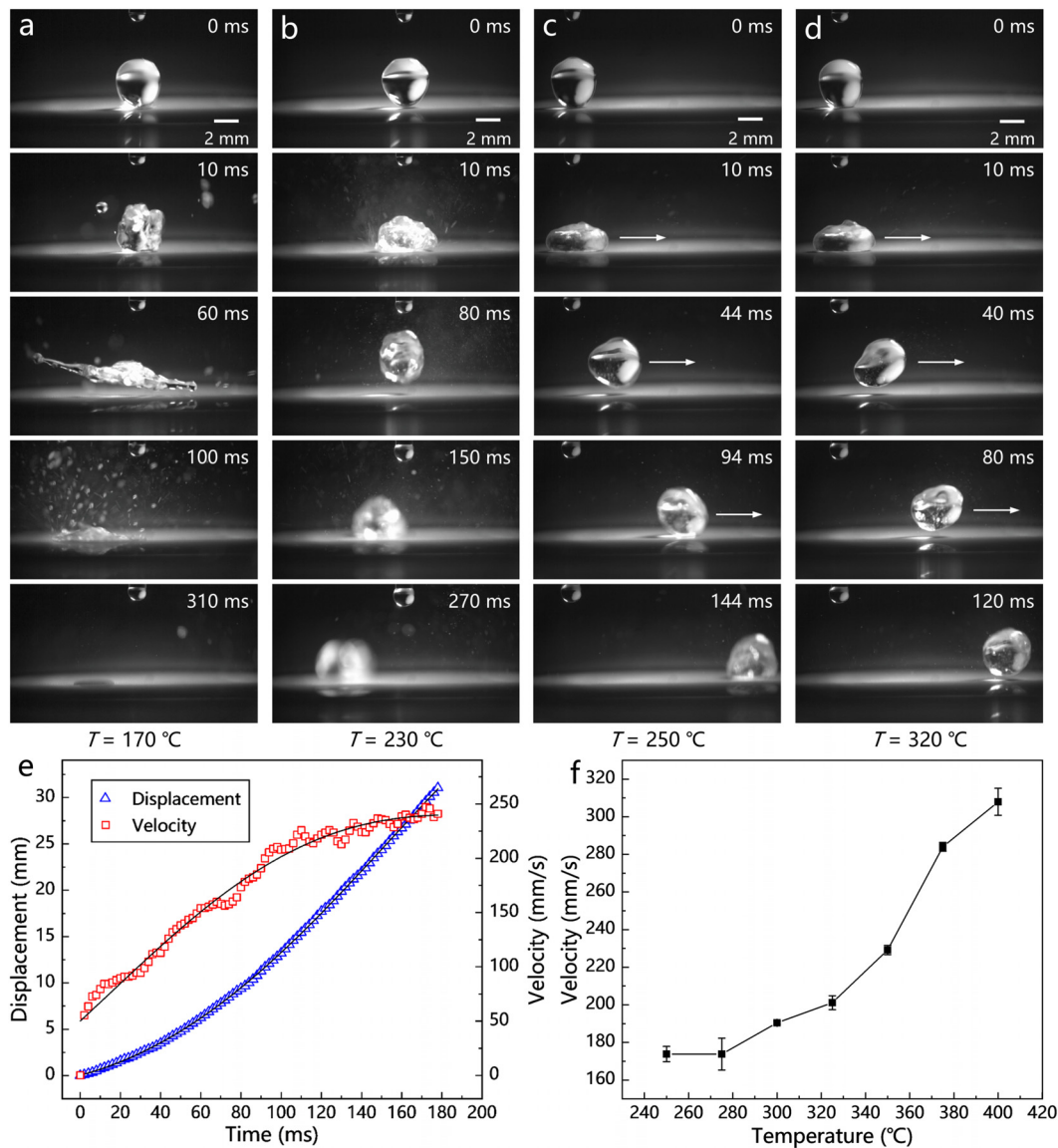


**FIG. 3.** Dynamic behavior of a droplet on the heated asymmetric microgroove array ( $\Lambda = 50 \mu\text{m}$ ). (a) Rapid *in situ* evaporation of a water droplet at 170 °C. (b) Water droplet in the transition boiling state and rolling randomly at 230 °C. (c) Water droplet starting to transport unidirectionally at 250 °C. (d) Droplet in the film boiling state at 320 °C. (e) Variation in the displacement and velocity of the droplet over time on the surface heated at 300 °C. (f) The velocity reached by the droplet after moving on the heated surface (at different temperatures) for 100 ms. (a)–(d). Multimedia available online.

droplets generated at the interface between the droplet and the substrate surface are violently ejected outward, and the resulting reverse thrust drives the droplet to begin to move across the surface. Due to the randomness of liquid ejection, the droplet rolls randomly in any direction, i.e., its movement is nondirectional. As the temperature increases to 250 °C and above, the motion direction of droplets becomes fixed, rather than random or omnidirectional. The droplet only moves along the positive direction (perpendicular to the parallel microgroove), as shown in Fig. 3(c). Figure 3(e) records the displacement and velocity of the droplet over time on the surface heated at 300 °C. The droplets move in the positive direction on the heated surface and gradually accelerate until they reach a stable velocity. A further increase in temperature makes the unidirectional movement of the droplets more significant. For example, a droplet moves faster on asymmetric microgrooves at 320 °C [Fig. 3(d)] than at 250 °C. Figure 3(f) shows the velocity reached by the droplets after moving on the heated surface (at different temperatures) for 100 ms. It can also be seen that the higher the heating temperature is, the greater the velocity that the droplets can obtain. The droplet velocity can even exceed 318 mm/s at 400 °C. Even when the substrate is slightly inclined, the Leidenfrost droplets can overcome gravity and climb up the inclined

surface, exhibiting strong unidirectional mobility [Fig. 1(i) and Movie S1 in the Multimedia available online].

As shown in Fig. 4(a), unidirectional droplet transport can only be achieved on asymmetric microgrooves with  $\Lambda = 50 \mu\text{m}$  (fabricated at laser power of 250 mW and scanning speed of 2 mm/s) when  $T$  is higher than 245 °C. The droplet has no directional motion characteristic on the surfaces with other  $\Lambda$  values because there is no obvious asymmetric microgroove structure on these surfaces [Figs. 1(e)–1(h)]. Droplets of different sizes (10–30  $\mu\text{l}$ ) can achieve unidirectional motion on the asymmetric microgrooves ( $\Lambda = 50 \mu\text{m}$ ). With the increase in the droplet volume, the critical temperature changing from the nucleate boiling state to the transition boiling state slightly increases, while the critical temperature at which the droplet develops unidirectional motion basically remains unchanged [Fig. 4(b)]. The initial volume of the droplet has little effect on the realization of unidirectional motion, because the size of the droplet is much larger than that of the microgroove. The upward tilt of the substrate will increase the resistance of the Leidenfrost droplet to directional motion. On inclined surfaces, higher surface temperatures are needed to achieve unidirectional droplet movement [Fig. 4(c)]. Asymmetric microgrooves can allow droplets to climb even surfaces that are tilted 14°,

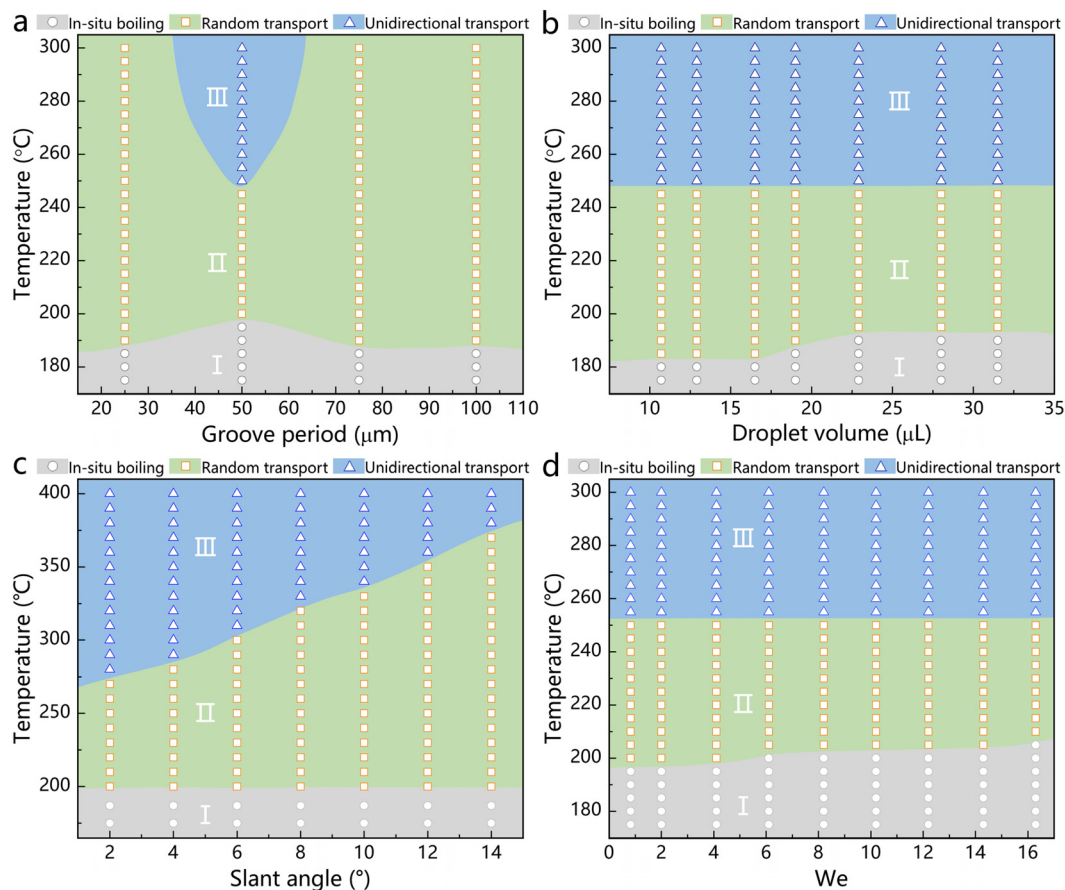


**FIG. 4.** Phase diagram showing the influence of (a) the period of the microgroove array, (b) the volume of the droplet, (c) the tilt angle of the substrate, and (d) the Weber number on the droplet's kinetic behavior on the heated asymmetric microgrooves. The droplets exhibit three different states on the heated surface: (I) *in situ* evaporation (labeled gray), (II) random transport (labeled green), and (III) unidirectional transport (labeled blue).

such a large climbing angle has rarely been achieved by macroscopic ratchets. The Weber number is a dimensionless value used to compare the kinetic energy and surface energy of a droplet. It is defined as  $We = \rho_l U_d^2 R / \gamma$ , where  $\rho_l$ ,  $U_d$ ,  $R$ , and  $\gamma$  are the liquid density, droplet falling velocity, equatorial radius, and surface tension of the droplet, respectively. Figure 4(d) shows that the Weber number has little effect on the critical temperature at which the droplet begins unidirectional transport. In our experiment, the Weber number is adjusted by releasing droplets at different heights. Therefore, whether the droplet is dropped from a low place or a high place, when the surface temperature exceeds the same critical value, the droplet will move in a fixed direction on the laser-induced asymmetric microgrooves.

Several mechanisms have been proposed to explain the unidirectional motion of Leidenfrost droplets or solids on a macroscopic 3D asymmetric surface, such as Linke's viscous mechanism of vapor,<sup>17</sup> Lagubeau's "rocket effect,"<sup>19</sup> Wurger's thermal creep mechanism,<sup>18</sup> and Dupeux's viscous mechanism model.<sup>39</sup> In general, the directional motion of droplets on asymmetric structures is mainly based on a viscous mechanism. The vapor cushion ejected from the bottom of the Leidenfrost droplet is able to overcome its own gravity and suspend the droplet on the substrate surface. The asymmetric structure can rectify the water vapor and generate a viscous shear force at the bottom of the droplet, making the droplet move under the action of the uneven force.

Figure 5 shows a schematic of a water droplet on the heated asymmetric microgroove array. Since the width of the laser-induced microgroove is much smaller than the size of the droplet, the deformation of the bottom surface of the droplet on the microgroove is negligible. Thus, the bottom surface of the droplet can simply be seen as a flat surface, similar to a Leidenfrost solid.<sup>40</sup> The droplet used in our experiment is smaller than the capillary length, so the contact radius ( $r_c$ ) at

the bottom of the droplet can be estimated as  $r_c \sim R^2/l_c$ , where  $l_c \sim \sqrt{\gamma/\rho_l g}$  is the capillary length for water and  $g$  is the acceleration of gravity.<sup>6,40</sup> The evaporation process of the bottom surface of a droplet on the heated asymmetric microgrooves follows the conservation of mass:  $\dot{m} \sim \rho_v h_0 r_c U$ , where  $\dot{m}$  is the mass of the gas ejected per unit time,  $\rho_v$  is the density of vapor,  $h_0$  is the gap between the bottom surface of the droplet and the microgroove surface, and  $U$  is the radial gas velocity.<sup>7,19,40</sup> The pressure exerted by the droplet on the vapor layer can be approximated as  $\Delta P \sim \frac{Mg}{r_c^2} \sim \frac{\rho_l R^2 g}{r_c^2} \sim \frac{\gamma}{R}$ , where  $M$  is the mass of the droplet.<sup>40</sup> In addition, according to an approximate lubrication theory,<sup>7,39,40</sup> the vapor flow follows  $\frac{\Delta P}{r_c} \sim \frac{\mu_v U}{h_0^2}$  (where  $\mu_v$  is the vapor viscosity). Based on the above-mentioned formulas, the vapor mass flow rate can be expressed as

$$\dot{m} \sim \frac{\rho_v \gamma h_0^3}{\mu_v R}. \quad (1)$$

The energy of the droplet remains conserved during the steady evaporation phase. When the droplet temperature reaches the saturation value,  $T_{sat}$ , the heat absorbed at the bottom of the droplet is mainly used for phase transition. According to the conservation of energy, there is the following energy conversion formula:<sup>7,19,40</sup>

$$\dot{m}L \sim \frac{k_v(T - T_{sat})r_c^2}{h_0}, \quad (2)$$

where  $L$  is the water latent heat of evaporation,  $k_v$  is the thermal conductivity, and  $T$  is the temperature of Al substrate. Combined with Eqs. (1) and (2), the thickness of the vapor film can be expressed as

$$h_0 \sim \left( \frac{k_v \mu_v \rho_l g (T - T_{sat})}{L \rho_v \gamma^2} \right)^{\frac{1}{3}} R^{\frac{5}{3}}. \quad (3)$$

Compared with the traditional ratchet structure, the asymmetric microgroove structure is different in two aspects: scale and symmetry degree. Since the depth of the traditional ratchet is much greater than the thickness of the vapor film at the bottom of the droplet, and the structure is completely asymmetrical, it can be considered that the vapor flow flows almost mainly along the slope with small inclination.<sup>19</sup> Regarding to the microgroove structure, the depth ( $H$ ) of the microgrooves is close to the thickness of the vapor film ( $h_0$ ), and the degree of asymmetry of the microridges is relatively weak. As shown in Fig. 5, the downward jet of vapor from the bottom of the droplet is rectified by the asymmetric microgrooves and flows along both slopes of the microgrooves at approximately equal flow rates.<sup>19</sup> The radial vapor velocity on the side of the slope with a smaller inclination angle ( $\alpha$ ) is defined as  $U_+$ , and its flow direction is consistent with the positive direction. The vapor flow will accordingly generate a positive-directional viscous shear force ( $f_{d+}$ ) in the  $L_1$  area at the bottom of the droplet. The radial vapor velocity on the side of the slope with a larger inclination angle ( $\beta$ ) is defined as  $U_-$ . Similarly, the vapor will generate a negative-directional viscous shear force ( $f_{d-}$ ) in the  $L_2$  area at the bottom of the droplet. The  $U$  mentioned above is the generalized radial gas velocity, and the value  $U \approx U_+ \approx U_- \sim \frac{\Delta P h_0^2}{r_c \mu_v} \sim \frac{\gamma h_0^2}{r_c R \mu_v}$ . The  $f_{d+}$  is approximately  $f_{d+} \sim \frac{\mu_v U_+ r_c L_1}{h} = \frac{\mu_v U_+ r_c H}{h} = \frac{\mu_v U_+ r_c H}{h \tan \alpha}$ , where  $h = h_0 + H$ .<sup>7,19,39</sup> The  $f_{d-}$  is approximately  $f_{d-} \sim \frac{\mu_v U_- r_c L_2}{h} = \frac{\mu_v U_- r_c H}{h} = \frac{\mu_v U_- r_c H}{h \tan \beta}$ . The resultant force of viscous shear force generated by a single microgroove on the droplet is ( $f_{d+} - f_{d-}$ ). The total number of microgrooves covered by a droplet

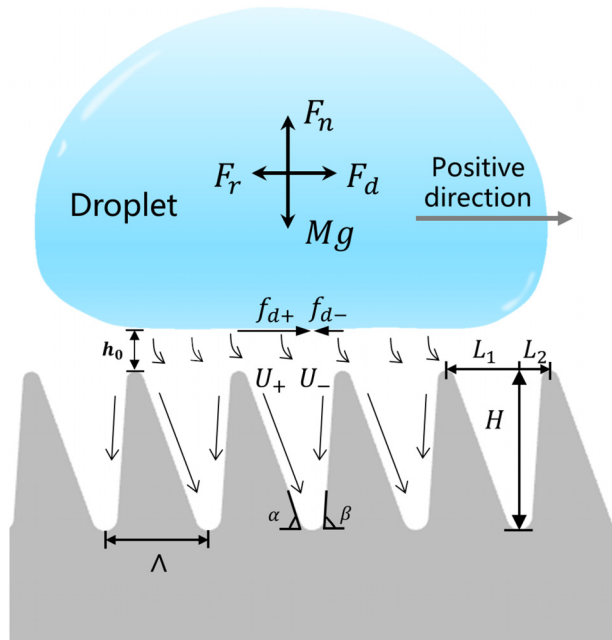


FIG. 5. Schematic of a water droplet on the heated asymmetric microgroove array and force analysis of the droplet.



is  $N = 2r_c/\Lambda$ . Thus, the total driving force ( $F_d$ ) of the droplet can be expressed as

$$F_d = N(f_{d+} - f_{d-}) \sim \frac{Hh_0^2R\sqrt{\gamma\rho_l g}}{(h_0 + H)\Lambda} \left( \frac{1}{\tan \alpha} - \frac{1}{\tan \beta} \right). \quad (4)$$

Since  $\alpha < \beta$ , so  $F_d > 0$ . On the heated asymmetric microgroove array, the adhesion between the Leidenfrost droplets and substrate is extremely low because the generated vapor steam lifts the droplets and the droplets no longer touch the solid surface, so this driving force makes it easy for the droplets to move.  $F_d > 0$  means that the droplet movement direction is in the positive direction, showing unidirectional motion. Assuming the radial velocity  $U \approx 10$  cm/s (according to Dupeux's measurement<sup>39</sup>), the average thickness of the vapor layer on the surface of the microgrooves is estimated to be approximately 32  $\mu$ m. The Reynolds number ( $Re$ ) can be calculated as  $\sim 0.27$ . The Reynolds number is in the low range, which indicates that the viscosity mechanism of the vapor is dominant, further verifying the validity of this explanation<sup>40,41</sup> (see the supplementary material for more details).

As shown in Fig. 5, the droplet is affected by four main forces. In the vertical direction, the supporting force ( $F_r$ ) provided by the downward jet of vapor from the droplet bottom is balanced with the droplet gravity ( $Mg$ ). In the process of horizontal motion, the resistance of Leidenfrost droplet movement mainly comes from the surrounding air. According to Stoke's friction law (the typical value of the Reynolds number is low), the drag force ( $F_r$ ) will depend linearly on the droplet's velocity:<sup>17,40</sup>  $F_r \sim -kv_x(t)$ , where  $v_x(t)$  is the horizontal velocity of the droplet,  $t$  is the time, and  $k$  is the friction coefficient. According to Newton's second law, the droplet velocity will consequently satisfy the following ordinary differential equation:

$$M \frac{dv_x(t)}{dt} = F_d - kv_x(t). \quad (5)$$

The droplets on the heated asymmetric microgrooves will be accelerated until reach a terminal velocity  $v_t = \frac{F_d}{k}$  when  $\frac{dv_x(t)}{dt} = 0$ .

It is found that the transport direction of the Leidenfrost droplets on the asymmetric microgrooves is the same as the direction of the adding of the laser scanning lines, i.e., the positive direction. Therefore, the direction of droplet movement can be flexibly designed by the distribution and processing sequence of laser scanning lines. Even with the same scanning line distribution, different processing sequences will lead to different directions of droplet motion. For example, the positions of the laser scanning lines in Figs. 6(a) and 6(b) are exactly the same. The scanning lines in Fig. 6(a) are processed from both sides to the middle, while the scanning lines in Fig. 6(b) are processed from the middle to the sides. When a water droplet is randomly dropped on the structured surface, the droplet moves toward the middle in Fig. 6(a) and toward the sides in Fig. 6(b) (Movie S6, Multimedia available online). For the asymmetric microgrooves with concentric ring distribution (Movie S6, Multimedia available online), when the laser scanning lines are processed from the outside to the center, the resultant texture can realize the convergent movement of the droplets (transporting toward the center of the ring) [Fig. 6(c)]. On the contrary, processing from the center to the outside can achieve divergent movement of the droplets (transporting away from the center) [Fig. 6(d)]. In addition to the straight line movement, the structural design can also make the Leidenfrost droplets turn. For example, Fig. 6(e) shows an "L"-shaped trajectory consisting of periodic small segments of microgroove arrays arranged in sequence at 1 mm intervals. The embedded unablated area is designed to prevent the droplets from

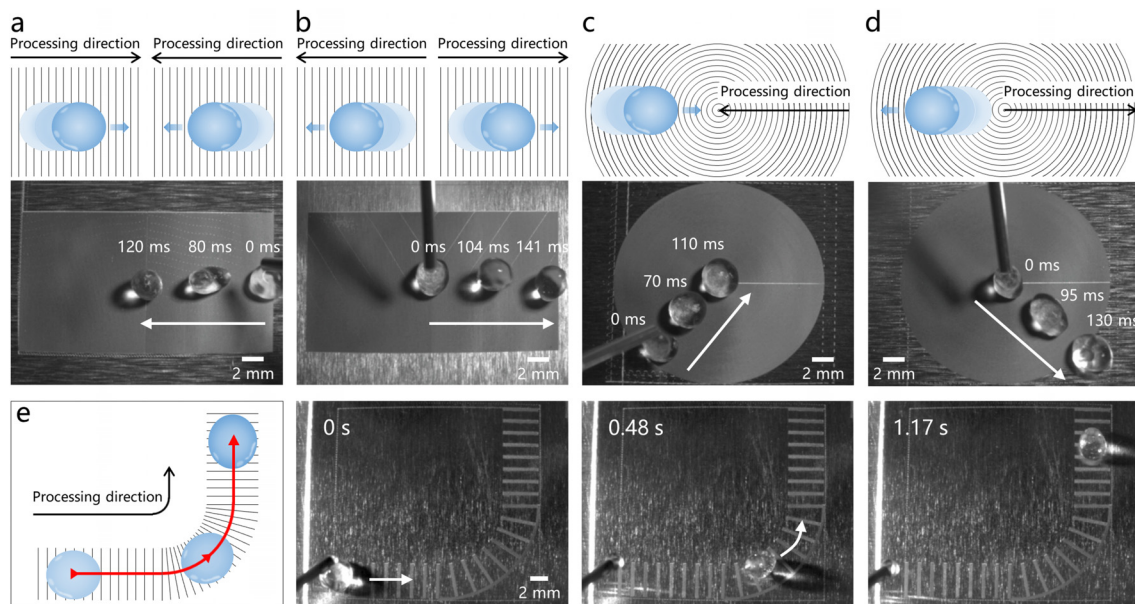


**FIG. 6.** Designable motion of Leidenfrost droplets on the laser-induced asymmetric microgroove arrays. (a) and (b) Different motion directions of Leidenfrost droplets on the same scanning line distribution (parallel microgrooves): (a) the scanning lines are added from both sides to the middle and (b) the scanning lines are added from the middle to the sides. (c) Convergent movement and (d) divergent movement of droplets on the asymmetric microgrooves with concentric ring distribution. (e) Droplet following a designed L-shaped trajectory to achieve 90° turning transport. Multimedia available online.



moving too fast and becoming difficult to control. The droplet can follow this trajectory to achieve 90° turning transport (Movie S6, Multimedia available online). These results show that the motion of Leidenfrost droplets on the femtosecond laser-written asymmetric microgrooves can be well designed, which is difficult to achieve on traditional macroscopic ratchet structures.

Combined with the flexibility of the femtosecond laser in the design of surface micro/nanostructures and the unidirectional fast

motion of Leidenfrost droplets on laser-induced asymmetric microgrooves, complex control of droplet motion can be achieved by designing different patterned structures. Figure 7(a) and Movie S7 (Multimedia available online) show a surface pattern in which a droplet can be manipulated to move in a circle. The outer circle region is composed of a concentric asymmetric microgroove array, with the microridges tilting away from the center. This region can drive the Leidenfrost droplets toward the center. The inner circle is also a

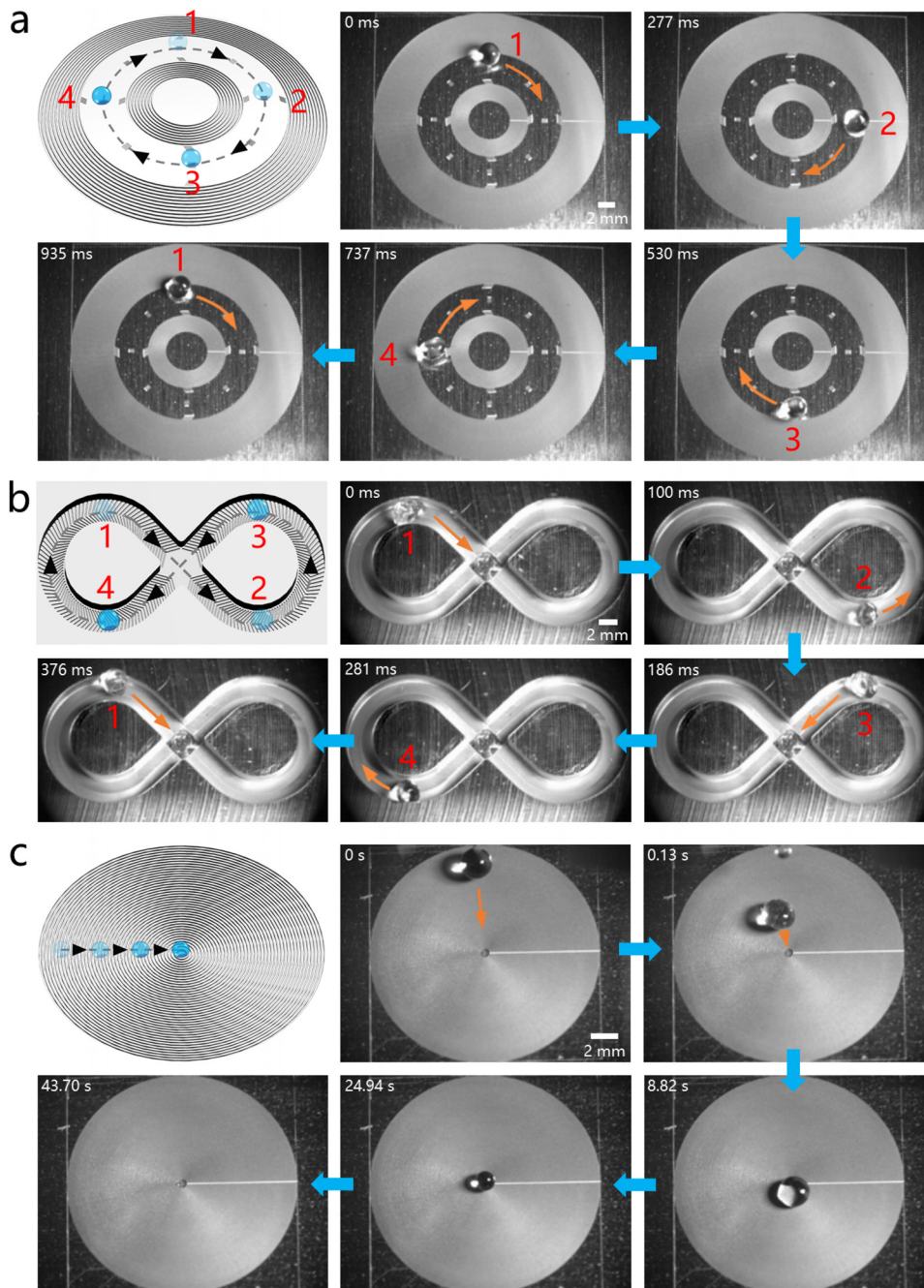


**FIG. 7.** Various droplet manipulation applications based on unidirectional droplet motion on heated asymmetric microgroove arrays. (a) Spontaneous motion along a designed trajectory (e.g., moving in a circle). (b) Droplet accelerator device where the droplet will continue to be accelerated. (c) Fixed-point trapping and evaporating of droplets for potentially achieving fixed-point cooling of hot solid surfaces. The orange arrows indicate the moving direction of the droplet. The first image is the schematic diagram, and the remaining images are the time-lapse sequences of the experimental results. Multimedia available online.

concentric microgroove array, while the inclination direction of the microridges is toward the center. The droplets in this region will move away from the center of the circle. Thus, droplets on the heated surface can be effectively confined to the region between the inner and outer rings. Furthermore, some small area microgroove arrays are inserted in the middle region, which can provide driving source. The droplet is able to spontaneously push forward along the defined ring for at least ten cycles. Therefore, through the design of the surface microstructures and patterns by the femtosecond laser, we can realize the controllable spontaneous movement of the droplet along the designed trajectory.

Continuous droplet acceleration can be achieved by using the driving effect of the asymmetric microgrooves and the unlimited movement distance of the Leidenfrost droplet. Figure 7(b) and Movie S8 (Multimedia available online) show a designed droplet accelerator device where uniform asymmetric microgrooves are prepared at the bottom of a “∞”-shaped macroscopic square groove with a width of ~3 mm and a depth of ~2 mm. When a droplet is released into the square groove (at 300 °C), the droplet is driven by the asymmetric microgrooves and moves along the ∞-shaped groove. The designed pattern has no end point for droplet movement, so the droplet will continue to be accelerated. After completing only one cycle, the motion speed of the droplet can reach 200 mm/s.

Figure 7(c) and Movie S9 (Multimedia available online) show a simple concentric circular asymmetric microgrooves that can drive the droplet to a specific target location on the hot surface. The direction of laser processing is from the outside to the center of the circle. When a droplet is released anywhere on the sample surface, it will spontaneously roll toward the central region. After undergoing a motion similar to a damped oscillation, the droplet eventually stays in the central trap region. The droplet seems to be attracted to the central region and trapped. As the droplet absorbs heat during the rapid evaporation process, it cools the central region of the Al substrate, achieving fixed-point cooling of the hot surface to a certain extent.

In conclusion, we found unidirectional droplet motion on the heated asymmetric microgroove arrays. The asymmetric microgrooves can be directly written by a femtosecond laser. On the heated surface, the asymmetry of the microgrooves can rectify the water vapor and generate a viscous shear force at the bottom of the droplet. When the temperature of the structured surface is higher than a certain critical value (threshold value), the droplets only roll along the positive direction under the action of the uneven driving force, showing strong unidirectional motion. The velocity of droplets can exceed 318 mm/s, and the droplets can even climb surfaces that are tilted 14°. Spontaneous and unidirectional droplet motions can support a variety of complex droplet-manipulation applications, such as droplet movement along designed trajectories, droplet accelerator devices, fixed-point capture of droplets, and fixed-point cooling of hot solid surfaces. The femtosecond laser has the characteristic of high flexibility in the design of surface microstructures and patterns. Compared with the traditional macroscale ratchet structure, the femtosecond laser-induced asymmetric microgrooves are simpler and more designable, so they can realize many functions that are difficult to achieve with the macroscale ratchet.

See the supplementary material for the details on the formation of the asymmetric microgrooves, the dynamic behavior of droplets on the heated smooth Al surface and homogeneous nanostructured surface, and movies of the dynamic process of droplet motion.

This work was supported by the USTC Research Funds of the Double First-Class Initiative (Nos. YD2090002013 and YD234000009) and the National Natural Science Foundation of China (Nos. 61927814, 62325507, 52122511, U20A20290, and 62005262). We acknowledge the Experimental Center of Engineering and Material Sciences at USTC for the fabrication and measurement of the samples. This work was partly carried out at the USTC Center for Micro and Nanoscale Research and Fabrication.

## AUTHOR DECLARATIONS

### Conflict of Interest

The authors have no conflicts to disclose.

## Author Contributions

**Zilong Cheng:** Conceptualization (equal); Data curation (equal); Formal analysis (equal); Investigation (equal); Writing – original draft (equal). **Chaowei Wang:** Funding acquisition (equal); Writing – review & editing (equal). **Xinlei Li:** Investigation (supporting). **Tianyu Xu:** Investigation (supporting). **Zhenrui Chen:** Investigation (supporting). **Zehang Cui:** Investigation (supporting). **Kangru Cheng:** Investigation (supporting). **Suwan Zhu:** Investigation (supporting); Visualization (supporting). **Dong Wu:** Funding acquisition (equal); Supervision (equal); Writing – review & editing (equal). **Jiale Yong:** Conceptualization (equal); Funding acquisition (equal); Project administration (equal); Supervision (equal); Writing – original draft (equal); Writing – review & editing (equal).

## DATA AVAILABILITY

The data that support the findings of this study are available from the corresponding authors upon reasonable request.

## REFERENCES

- <sup>1</sup>L. L. Hou, X. F. Liu, X. R. Ge *et al.*, “Designing of anisotropic gradient surfaces for directional liquid transport: Fundamentals, construction, and applications,” *Innovation* **4**, 100508 (2023).
- <sup>2</sup>P. Lv, Y. L. Zhang, D. D. Han *et al.*, “Directional droplet transport on functional surfaces with superwettabilities,” *Adv. Mater. Interfaces* **8**, 2100043 (2021).
- <sup>3</sup>F. Y. Lin, K. Y. Wo, X. J. Fan *et al.*, “Directional transport of underwater bubbles on solid substrates: Principles and applications,” *ACS Appl. Mater. Interfaces* **15**, 10325–10340 (2023).
- <sup>4</sup>K. Ichimura, S. K. Oh, and M. Nakagawa, “Light-driven motion of liquids on a photoresponsive surface,” *Science* **288**, 1624–1626 (2000).
- <sup>5</sup>F. Wang, M. J. Liu, C. Liu *et al.*, “Light-induced charged slippery surfaces,” *Sci. Adv.* **8**, eabp9369 (2022).
- <sup>6</sup>A. Bouillant, T. Mouterde, P. Bourriane *et al.*, “Leidenfrost wheels,” *Nat. Phys.* **14**, 1188–1192 (2018).
- <sup>7</sup>A. Li, H. Z. Li, S. Lyu *et al.*, “Tailoring vapor film beneath a Leidenfrost drop,” *Nat. Commun.* **14**, 2646 (2023).
- <sup>8</sup>Q. Sun, D. Wang, Y. Li *et al.*, “Surface charge printing for programmed droplet transport,” *Nat. Mater.* **18**, 936–941 (2019).
- <sup>9</sup>D. Wu, Z. Zhang, Y. Y. Zhang *et al.*, “High-performance unidirectional manipulation of microdroplets by horizontal vibration on femtosecond laser-induced slant microwall arrays,” *Adv. Mater.* **32**, 2005039 (2020).
- <sup>10</sup>Y. Y. Zhang, J. Li, L. Xiang *et al.*, “A biocompatible vibration-actuated omnidirectional rectifier with large volume range fabricated by femtosecond laser,” *Adv. Mater.* **34**, 2108567 (2022).
- <sup>11</sup>H. Chen, T. Ran, Y. Gan *et al.*, “Ultrafast water harvesting and transport in hierarchical microchannels,” *Nat. Mater.* **17**, 935–942 (2018).

- <sup>12</sup>M. K. Chaudhury and G. M. Whitesides, "How to make water run uphill," *Science* **256**, 1539–1541 (1992).
- <sup>13</sup>J. Ju, H. Bai, Y. M. Zheng *et al.*, "A multi-structural and multi-functional integrated fog collection system in cactus," *Nat. Commun.* **3**, 1247 (2012).
- <sup>14</sup>Y. Li, Z. Cui, G. Li *et al.*, "Directional and adaptive oil self-transport on a multi-bioinspired grooved conical spine," *Adv. Funct. Mater.* **32**, 2201035 (2022).
- <sup>15</sup>I. U. Vakarelski, N. A. Patankar, J. O. Marston *et al.*, "Stabilization of Leidenfrost vapour layer by textured superhydrophobic surfaces," *Nature* **489**, 274–277 (2012).
- <sup>16</sup>J. C. Burton, A. L. Sharpe, R. C. A. Van Der Veen *et al.*, "Geometry of the vapor layer under a Leidenfrost drop," *Phys. Rev. Lett.* **109**, 074301 (2012).
- <sup>17</sup>H. Linke, B. J. Alemán, L. D. Melling *et al.*, "Self-propelled Leidenfrost droplets," *Phys. Rev. Lett.* **96**, 154502 (2006).
- <sup>18</sup>A. Würger, "Leidenfrost gas ratchets driven by thermal creep," *Phys. Rev. Lett.* **107**, 164502 (2011).
- <sup>19</sup>G. Lagubeau, M. Le Merrer, C. Clanet *et al.*, "Leidenfrost on a ratchet," *Nat. Phys.* **7**, 395–398 (2011).
- <sup>20</sup>T. R. Cousins, R. E. Goldstein, J. W. Jaworski *et al.*, "A ratchet trap for Leidenfrost drop," *J. Fluid Mech.* **696**, 215–227 (2012).
- <sup>21</sup>C. Liu, K. Sun, C. G. Lu *et al.*, "One-step process for dual-scale ratchets with enhanced mobility of Leidenfrost droplets," *J. Colloid Interface Sci.* **569**, 229–243 (2020).
- <sup>22</sup>J. L. Yong, Y. B. Peng, X. W. Wang *et al.*, "Self-driving underwater 'aerofluidics,'" *Adv. Sci.* **10**, 2301175 (2023).
- <sup>23</sup>J. L. Yong, Q. Yang, J. L. Huo *et al.*, "Underwater gas self-transportation along femtosecond laser-written open superhydrophobic surface microchannels (<100  $\mu\text{m}$ ) for bubble/gas manipulation," *Int. J. Extreme Manuf.* **4**, 015002 (2022).
- <sup>24</sup>J. L. Yong, Q. Yang, F. Chen *et al.*, "A simple way to achieve superhydrophobicity, controllable water adhesion, anisotropic sliding, and anisotropic wetting based on femtosecond-laser-induced line-patterned surfaces," *J. Mater. Chem. A* **2**, 5499–5507 (2014).
- <sup>25</sup>D. S. Zhang, R. J. Liu, and Z. G. Li, "Irregular LIPSS produced on metals by single linearly polarized femtosecond laser," *Int. J. Extreme Manuf.* **4**, 015102 (2022).
- <sup>26</sup>K. Sugioka and Y. Cheng, "Femtosecond laser three-dimensional micro- and nanofabrication," *Appl. Phys. Rev.* **1**, 041303 (2014).
- <sup>27</sup>A. Y. Vorobyev and C. L. Guo, "Direct femtosecond laser surface nano/micro-structuring and its applications," *Laser Photonics Rev.* **7**, 385–407 (2013).
- <sup>28</sup>E. Stratakis, J. Bonse, J. Heitz *et al.*, "Laser engineering of biomimetic surfaces," *Mater. Sci. Eng., R* **141**, 100562 (2020).
- <sup>29</sup>C. Kruse, I. Somanas, T. Anderson *et al.*, "Self-propelled droplets on heated surfaces with angled self-assembled micro/nanostructures," *Microfluid. Nanofluid.* **18**, 1417–1424 (2015).
- <sup>30</sup>J. Yong, Q. Yang, X. Hou *et al.*, "Nature-inspired superwettability achieved by femtosecond lasers," *Ultrafast Sci.* **2022**, 9895418.
- <sup>31</sup>X. Chen and M. Gu, "Two-beam ultrafast laser scribing of graphene patterns with 90-nm subdiffraction feature size," *Ultrafast Sci.* **2022**, 0001.
- <sup>32</sup>L. Zhu, Y.-L. Zhang, and H.-B. Sun, "Miniaturising artificial compound eyes based on advanced micronanofabrication techniques," *Light: Adv. Manuf.* **2**, 7 (2021).
- <sup>33</sup>M. N. Jiang, Y. Wang, F. Y. Liu *et al.*, "Inhibiting the Leidenfrost effect above 1,000 °C for sustained thermal cooling," *Nature* **601**, 568–572 (2022).
- <sup>34</sup>C. Liu, C. Lu, Z. C. Yuan *et al.*, "Steerable drops on heated concentric micro-groove arrays," *Nat. Commun.* **13**, 3141 (2022).
- <sup>35</sup>V. Talari, P. Behar, Y. Lu *et al.*, "Leidenfrost drops on micro/nanostructured surfaces," *Front. Energy* **12**, 22–42 (2018).
- <sup>36</sup>T. Tran, H. J. J. Staat, A. Prosperetti *et al.*, "Drop impact on superheated surfaces," *Phys. Rev. Lett.* **108**, 036101 (2012).
- <sup>37</sup>A. L. Bianco, C. Clanet, and D. Quere, "Leidenfrost drops," *Phys. Fluids* **15**, 1632–1637 (2003).
- <sup>38</sup>J. Li, Y. M. Hou, Y. H. Liu *et al.*, "Directional transport of high-temperature Janus droplets mediated by structural topography," *Nat. Phys.* **12**, 606–612 (2016).
- <sup>39</sup>G. Dupeux, M. Le Merrer, G. Lagubeau *et al.*, "Viscous mechanism for Leidenfrost propulsion on a ratchet," *EPL* **96**, 58001 (2011).
- <sup>40</sup>A. G. Marín, D. A. del Cerro, G. Römer *et al.*, "Capillary droplets on Leidenfrost micro-ratchets," *Phys. Fluids* **24**, 122001 (2012).
- <sup>41</sup>J. Li, X. F. Zhou, Y. J. Zhang *et al.*, "Rectification of mobile Leidenfrost droplets by planar ratchets," *Small* **16**, 1901751 (2020).